Exp Astron (2013) 35:507–526
DOI 10.1007/s10686-012-9320-3

ORIGINAL ARTICLE

Measurement of arrival time of particles in extensive air showers using TDC32

S. K. Gupta · J. Christiansen · Y. Hayashi · A. Jain · P. K. Mohanty · K. C. Ravindran · B. Satyanarayana

Received: 1 August 2012 / Accepted: 26 September 2012 / Published online: 13 October 2012

Abstract Arrival time of particles in an extensive air shower (EAS) is a key physical parameter to determine its direction. EAS direction is useful for studies of anisotropy and composition of cosmic rays, and search for multi-TeV γ-rays sources. Accurate timing may be used to search exotic phenomena such as production of new particles at extremely high energies available during early stages of development of EAS and also for detecting sub-relativistic hadrons in EAS. Time to digital converters (TDCs) are used to perform this task. Traditional TDCs operate in the START-STOP mode with limited dynamic range and single-hit capability. With the advent of high luminosity collider LHC, need for TDCs with large dynamic range, multi-hit capability and TRIGGERED mode of operation became necessary. A 32 channel TDC was designed for the GRAPES-3 experiment on a CAMAC platform around TDC32, an ASIC developed by micro-electronics group at CERN, Geneva. Four modules were operated in the GRAPES-3 experiment. Here, we present details of the circuit design and their performance over several years. The multi-hit feature of this device was used to study the time structure of particles in the EAS on time scale of $\sim$1 μs. The distribution of time intervals in the

S. K. Gupta · A. Jain · P. K. Mohanty · K. C. Ravindran · B. Satyanarayana
Tata Institute of Fundamental Research, Mumbai 400 005, India

S. K. Gupta (✉) · A. Jain · P. K. Mohanty · K. C. Ravindran · B. Satyanarayana
GRAPES–3 Experiment, Cosmic Ray Laboratory, Ooty 643 001, India
e-mail: gupta@grapes.tifr.res.in

J. Christiansen
Microelectronics Group, CERN, Geneva 23, Switzerland

Y. Hayashi
Faculty of Science, Osaka City University, Osaka 558-8585, Japan

multi-hit data shows an exponential profile with a time constant of ∼370 ns. These delayed particles are likely to be neutrons produced in the EAS core that were recorded in the scintillator detectors following the relativistic EAS front.

Keywords Cosmic rays · Extensive air showers

1 Introduction

An overwhelming fraction of the high energy cosmic rays are charged particles that are deflected by interstellar magnetic fields during their propagation in the galaxy. The random orientation of galactic magnetic field effectively converts the motion of cosmic rays into diffusion. This results in a total loss of information on the direction their sources. Thus, the only option available to directly identify the cosmic ray sources is to detect the photon (γ-ray) component that travels in a straight line, unaffected by interstellar magnetic fields and thus preserving the source direction. Therefore, important knowledge of high energy processes leading to production and acceleration of cosmic rays to high energies may be obtained through the detection of cosmic γ-rays.

A large fraction of cosmic rays of energies below the '*knee*' are accelerated in supernovae explosions within the galaxy, mainly through diffusive shock acceleration [1]. This makes supernova remnants in the galaxy an important target for detection of high energy γ-rays. Pulsars are also capable of accelerating particles to high energies [2]. The CRAB pulsar and its nebula have been extensively studied at most wavelengths and the observations by satellite based detectors have established it as a *standard candle* from MeV to GeV energies. These observations imply the presence of highly relativistic electrons that have been accelerated to energies beyond hundreds of GeV. The existence of synchronous pulsed emission from radio (10^{-5} eV) to GeV γ-rays, underlines the importance of the CRAB pulsar in accelerating charged particles in the nebula [3].

Study of photon sources above 100 GeV requires large collection area and exposure time, that are presently possible only with ground based detectors employing the atmospheric Cherenkov technique (ACT) [3, 4]. However, the cosmic sources of yet higher energy ($\geq$10 TeV) γ-rays can only be studied using the extensive air shower (EAS) technique, that allows sufficiently large area and exposure time factors. Since the γ-ray flux from a source has to be detected against a massive background contributed by the isotropic flux of cosmic rays, the success of this technique critically depends on an effective rejection of this massive background. For a point source, the signal to background ratio is inversely proportional to the square of the angular resolution. Therefore, the most critical parameter in an EAS detector system is its angular resolution. The technique of relative arrival time has been widely used in EAS arrays for determining the arrival direction of showers [4–7].

Study of EAS at energies below 100 TeV involves detection of shower electrons that suffer significant scattering in the atmosphere, prior to detection at ground level. Therefore, the angular resolution attainable in an EAS array is relatively poor as compared to an ACT that detects Cherenkov photons. Furthermore, the angular resolution of an EAS array also depends on the shower size at detection level and improves with increasing shower size. The best possible angular resolution may be achieved by deploying a carpet of detectors to maximize detected number of EAS particles and MILAGRO and ARGO-YBJ experiments are examples of this approach. The MILAGRO experiment had instrumented a 8 m deep water pond of 80×60 m^2 area, to detect Cherenkov photons produced by EAS particles inside water by photomultipliers (PMTs) [8]. The ARGO-YBJ experiment detects particles by a carpet of resistive plate chambers, covering an area of 74×78 m^2 [9]. Since the total carpet area in both experiments is < 6000 m^2, hence the sensitivity of these experiments peaks below 5 TeV.

In an alternative approach, the angular resolution may be improved by decreasing the inter-detector separation in an array. This strategy provides a reasonable compromise between a small area carpet array and a large area sparsely instrumented array. However, practical constraints imposed by logistical and funding considerations limit the total number of detectors deployed in an array. Further, an array provides only a sampling of particle density in an EAS. For example, in the Tibet ASγ [10], CASA-MIA [11], EAS-TOP [12], KASCADE [13], GAMMA [14] arrays, the physical area covered by detectors is $\leq$1 % of the total area of the array. The fraction of physical area covered by detectors in an array is a key factor that determines the angular resolution, which is critically important in search of γ-rays at multi-TeV energies. With these definitive considerations in mind, the GRAPES-3 (**G**amma **R**ay **A**stronomy at **P**eV **E**nergy**S** Phase-**3**) was designed to have one of the most compact configuration in a conventional EAS array, with a separation of only 8 m between adjacent detectors. The GRAPES-3 detectors are deployed in a symmetric hexagonal geometry, with a coverage of $\sim$2 % of total area of the array [7, 15].

The energy dependent angular resolution and the absolute pointing accuracy of the GRAPES-3 array was measured using three different methods that included, the even-odd, left-right and the Moon shadow technique. The even-odd method provides a quantitative estimate of the best achievable angular resolution as a function of shower size. The left-right method provides a measure of the shower front curvature and also serves as an independent measure of the angular resolution. In the third method four years of observations were used to obtain the shadow of Moon at a significance level of $\sim 5\sigma$. The Moon shadow besides providing an estimate of the angular resolution. Being caused by a celestial object it also yielded the absolute pointing accuracy of the array. Nearly identical values of the energy dependent angular resolution obtained by these three independent techniques indicates the reliability of these measurements. The angular resolution of the GRAPES-3 array is 1.4° at 10 TeV that steadily improves to 0.5° at 80 TeV [7].

For an incident EAS, the shower particles reach a given detector at a time, based on detector location and the EAS direction. For an EAS traveling along a direction θ, ϕ, the particles reach the detector located at **r** at a time **r.n**/c, relative to the origin of the co-ordinate frame. Here, the unit vector **n** is along θ, ϕ and the velocity of EAS particles was assumed to be the velocity of light c. Thus, in principle, if the arrival times at a minimum of three detectors were known, the unknown EAS direction (θ, ϕ) could be obtained from the arrival time data. The error in the measurement of arrival angle $\Delta\theta \sim c\Delta t/d$, where Δt is the error in time and d is the inter-detector distance. Therefore, accurate measurement of time is critically important for obtaining a good angular resolution. A time to digital converter (TDC) serves as the basic device that measures the arrival time of particles in each detector relative to the EAS trigger.

In addition, the TDCs with a multi-hit capability may be used to study the time structure of particles in the shower front. The shower front primarily comprises of relativistic particles that includes leptons and hadrons traveling at nearly the velocity of light. However, the neutrons produced in the shower core, being electrically neutral and possessing a very long lifetime (882 s) can travel large distances even at relatively low energies of $\sim$ sub-GeV. The presence of such sub-relativistic neutrons as a potential source of delayed particles in the EAS was anticipated a long time back [16]. The first indication of neutrons being the particles delayed by several μs relative to the EAS front came from some of the early experiments [17]. Recent measurements on delayed neutrons in the EAS have been extensively discussed in [18]. Using the data from neutron monitors operated along with the Tien-Shan array presence of delayed neutrons was reported with delays ranging from hundreds of μs to several ms possibly due to thermalization during the detection process [19]. However, the neutrons produced in the atmosphere follow the EAS front with delays of only a few μs. The detection of neutrons offers another independent method to identify the hadronic nature of the primary particle that may be used for a better hadron to γ separation.

The GRAPES-3 experiment consists of a dense array of plastic scintillator detectors and a large area tracking muon detector. The array at present consists of about 400 plastic scintillator detectors (each 1 m^2). These detectors are deployed with an inter-detector separation of 8 m. The array is being operated at Ooty in India (11.4°N, 76.7°E, 2200 m altitude) [15]. The total area of tracking muon detector is 560 m^2 with an energy threshold of 1 GeV in the vertical direction [20]. In Section 2 the operational characteristics of some of the conventional TDCs and that of the TDC32 are discussed. In Section 3 a brief description of the CAMAC printed circuit board designed to house the TDC32 is given. The performance of two commercially available TDCs, namely, Phillips Scientific of USA and Hoshin of Japan alongside TDC32 are compared in Section 4. The measurements of the time distribution of delayed particles are summarized in Section 5. The conclusions of this study are presented in Section 6.

2 Time to digital converters

A TDC is used to measure the time interval between two digital pulses by converting it into a numerical count that may be stored and accessed for further analysis. Since, each scintillator detector in GRAPES-3 experiment measures the arrival time of particles in an EAS, a large number of TDC channels are required to perform this task. This requirement could, in principle, be met in a cost effective manner by employing TDC32. The TDC32 is an application specific integrated circuit (ASIC) that contains 32 channels and was developed by Microelectronics group at CERN, Geneva as a prototype TDC for the LHC experiments. Some of the unique capabilities of this ASIC include a large dynamic range, multi-hit, low latency, excellent stability and the flexibility to use different operational modes, including the START-STOP and TRIGGERED modes. TDC32 is programmed using standard JTAG protocol and various operational parameters can be easily changed as per the requirements of the experiment [21]. TDC32 achieves a resolution of 521 ps with a clock of 60 MHz. This resolution is perfectly suitable for the GRAPES-3 experiment, where shower particles are spread several ns in time.

Conventional TDCs available commercially, for example, LeCroy, USA [22], Phillips Scientific, USA [23] or Hoshin, Japan [24] generally operate in the START-STOP mode. This entails the generation of a common START (STOP) signal that must precede (follow) the signals to be measured. That in turn, necessitates the use of long delay cables to ensure a proper temporal sequencing of signals. The dynamic range of most of these TDCs is limited to 12 bits and their operation confined to the single-hit mode. Therefore, once a channel receives signal it stays dead until the data is read and/or cleared. This is a serious limitation, specially in high rate and/or noisy environments where even an unwanted/noise pulse arriving before the signal can result in the loss of real signal. Most of these commercial TDC modules also contain far fewer (8 or 16) channels than the TDC32.

The eight channel LeCroy TDC (model 2228A) employs Wilkinson rundown method to convert a time interval into charge by charging a capacitor using a constant current source for the duration of the time interval being measured. Thereafter, the stored charge is digitized [22]. The Phillips Scientific TDC (model 7186) implements 16 channels of time to amplitude conversion followed by a digitization section and CAMAC interface in a single width CAMAC module [23]. Phillips Scientific [23] and Hoshin [24] TDCs use the technique of successive approximation for digitization, resulting in a non-linear response as discussed later on in Section 4. Unfortunately, these TDCs also suffer from a rather high power consumption (0.1–1 W per channel), high latency because of slower conversion and in some cases the time resolution gets modified in the presence of magnetic field [25].

The availability of TDC32 with 32 channels offers a great opportunity to develop a TDC system that is relatively inexpensive and offers numerous advantages over the earlier commercial models. These advantages include, a

large dynamic range of 21 bits, multi-hit capability with a double-hit resolution of 15 ns, operation in both START-STOP and TRIGGERED modes, a low power consumption (∼10 mW per channel) and low latency. TDC32 works on an entirely different mechanism of time division with the help of an external clock of maximum frequency of 60 MHz. The corresponding time period of 16.67 ns is effectively divided by a factor of 32, resulting in a resolution of $16.67/32 = 0.52$ ns per count. The enhanced resolution is achieved with the aid of a chain of 32 delay elements that form a delay locked loop (DLL) [26, 27], where the basic frequency remains unchanged, but the phase is shifted using a delay element. The implementation of the DLL was achieved by using standard CMOS technology.

The DLL for the TDC32 contains 32 identical delay elements, a phase comparator and a charge pump. The input to the DLL is a 60 MHz clock. The delay of each element can be adjusted by a control voltage. In the locked state, the 32 elements in the loop produce 32 outputs of 60 MHz, that are delayed by an equal amount by successive elements, such that the total delay in the loop equals one clock period. The phase detector compares the phase between the 60 MHz input clock with the output at the end of the loop and adjusts the pump by changing the bias of each delay element by an identical amount to ensure that the total delay stays equal to one clock period. Thus, the DLL effectively divides one clock period into 32 equal parts. This information is encoded into 5 bits that are combined with the 16 bit coarse count to provide a 21 bit output. The jitter in time after reaching the locked state was minimized through a careful design effort, because a large jitter can effectively compromise the performance of the TDC. A finite amount of time is needed for the delay chain to reach a locked state. This time depends on the current used in the charge pump. A low current results in a longer time to reach the locked state, but leads to smaller jitter. On the other hand a higher current leads to a faster lock with larger jitter. The current for the charge pump may be controlled through a JTAG command [21].

3 CAMAC printed circuit board for mounting TDC32

The time resolution and offset in a conventional TDC such as the Phillips model 7186 or Hoshin model C021 tend to drift with time and also vary from channel to channel. Hence these TDCs have to be calibrated at regular intervals to measure this variation. For TDC32, the time resolution depends only on the stability of the 60 MHz clock and all 32 channels, in general, have an identical resolution. Both Hoshin and Philips TDCs possess a time resolution better than TDC32, but their dynamic range is very limited. In conventional TDCs, if multiple STOP signals arrive after the START, then only the first STOP is registered. But the TDC32 is capable of measuring time interval between a START and multiple STOPs. In TRIGGERED mode the TDC32 can be operated with a pre-programmed time window of acceptance

for START inputs. The advantage of this mode is that the long delay cable required in START-STOP mode for every detector is avoided. The TDC32 may be programmed using standard JTAG protocol to operate in different modes unlike the conventional TDCs.

In TDC32 the input and control signals utilize a TTL logic. Depending upon the needs to the experiment, the TDC32 may be programmed to write the data for the channels hit or for every channel. The data contain a 5-bit channel number and 21 bits of time information. The TDC32 may be programmed to provide data after subtracting the time of common START. If multiple hits occur, then the time of each hit is written in the event buffer along with the corresponding channel number. In the TRIGGERED mode, after an event of interest is identified, the time of occurrence prior to, or after the trigger can be recorded. This is accomplished by programming the TDC32 to search for events during a time window before or after the START pulse.

In general, electronic instrumentation used for particle detection involves measurement, control and data recording. A modular system that is compact, flexible, and operates at high speeds through a digital interface is highly desirable. The CAMAC (Computer Automated Measurement and Control) is an open-architecture IEEE standard 583 that is non-proprietary and used worldwide. CAMAC incorporates an easy to implement mechanical and electrical specifications. One TDC32 ASIC was mounted on a printed circuit board (PCB) placed inside a double width CAMAC module, hereafter called 'G3TDC' module. The CAMAC DATAWAY powers the G3TDC module and also serves to address, control and bus the data using standard CAMAC commands. The benefits of this modular design include compactness, easy replacement of faulty modules and the flexibility to upgrade the design in future. The choice of CAMAC was dictated by its widespread use in the GRAPES-3 data acquisition system (DAQ). The station number, selected by an on-board DIP switch, indicates the location of a given G3TDC module in a crate, the address lines differentiate between channels and the function code performs specific operations including the READ, WRITE, CLEAR etc. The data from each channel are read into the controller during the READ operation and then stored in a memory buffer interfaced to the data storage computer.

The TTL logic is used for control and input/output operations since the TDC32 also utilizes this logic for various operations. Since most of the control electronics in the GRAPES-3 experiment is also based on TTL, its implementation in G3TDC posed no problems. The JTAG signals used to program the TDC32 after the power is switched on, are differential TTL, because these signals have to drive a relatively long cable ($\sim$4 m), they are converted into normal TTL, just before programming the TDC32. Similarly, the output signals from TDC32 drive TTL buffers en-route to the CAMAC controller. The control signals for the output buffers are generated in the control circuit segment of the PCB. A provision was made to daisy chain the JTAG programming signals from one to the next board for the ease of programming a number of G3TDC modules.

A two layer PCB was designed for mounting the TDC32 in a CAMAC module. The PCB houses, one TDC32 (84 pin PLCC), one Isplsi-PAL (32 pin PLCC) and a few additional ICs. In view of the presence of a relatively high frequency (60 MHz) clock, the layout of the components and the routing of the tracks was carried out with considerable care, specially since the high frequency clock can generate ripples on the power lines that can adversely impact the operation of TDC32. A separate +5 V isolated supply was provided on the PCB along with decoupling capacitors for each IC. 50Ω impedance RG-174 co-axial cables were used to propagate the 60 MHz clock and the shield in the co-axial cable was grounded to minimize potential electrical interferences. The 32 inputs of TDC32 were fed via 64 pins of two FRC connectors mounted on the front panel of the G3TDC module. These signals carry arrival time information of particles in a detector. The routing of STOP signals to the input buffer leading into TDC32 was done by maintaining similar track lengths to minimize potential time offsets in the PCB. A majority of the tracks were routed on the solder side and the unused area on the component side was covered with ground plane to further reduce the electrical noise.

Functionally, a G3TDC module consists of one TDC32 as the core component, a CONTROL UNIT, INPUT BUFFER, OUTPUT LATCH and a JTAG interface. A block diagram of G3TDC module is shown in Fig. 1. After the power is switched on, the JTAG interface programs the TDC32 and that includes the selection of, (i) the operating mode (TRIGGER or START-STOP), (ii) rising or falling edge of signal for timing, (iii) enable and/or disable

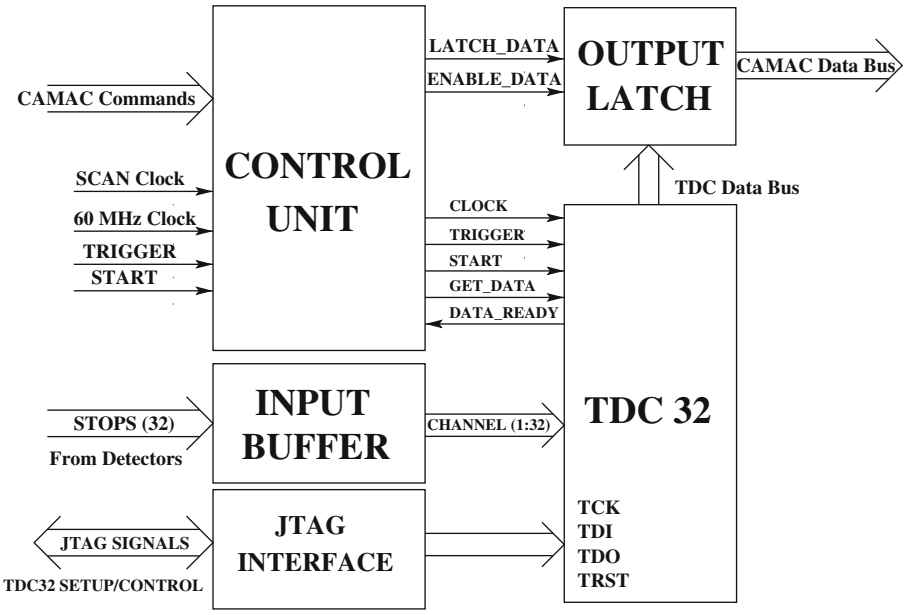

Fig. 1 Block Diagram of CAMAC based G3TDC

specific channels and so on. The JTAG setup functions are executed through four lines, namely, TCK (clock), TDI (input), TDO (output) and TRST (reset) as shown in Fig. 1. The CONTROL unit provides the interface with the external world and controls the access for reading the TDC32 data. The TDC32 receives the TRIGGER or START through the CONTROL UNIT that also inputs 60 MHz clock for the conversion of data in enabled channels. The STOP pulses from the GRAPES-3 detectors are buffered through the INPUT BUFFER into the TDC32 and upon the receipt of the TRIGGER the data are latched and loaded into the OUTPUT LATCH, after due handshake involving GET_DATA and DATA_READY commands. A command from the CAMAC controller initiates the transfer of the latched data into the CAMAC bus, by making use of the 1 MHz GRAPES-3 DAQ SCAN clock. Once the data are processed by the TDC32, then a DATA_READY signal is set to HIGH state indicating that the data are ready to be read from the 256 byte internal buffer of the TDC32.

The entire operation of the CONTROL UNIT is implementing by a careful sequencing of various steps with the aid of an elegant and simple hardwired logic using only seven flip flops, hereafter called FF1 through FF7, and a few basic gates as shown in Fig. 2. The SCAN clock is propagated when the CAMAC station housing a G3TDC module is enabled through an N_LINE. The change of state of various FFs due to passage of SCAN clock results in the generation of timing waveforms as shown in Fig. 3. The operation of the CONTROL UNIT may be understood by a closer examination of Fig. 2 in conjunction with Fig. 3. The rising edge of the SCAN clock sets FF1, alternatively to HIGH and LOW states, every 1 μs, as seen from the two complementary waveforms i.e. the 3rd and 4th from top in Fig. 3. The data for each channel contains a total of 32 bits (21 = 16 coarse + 5 fine bits

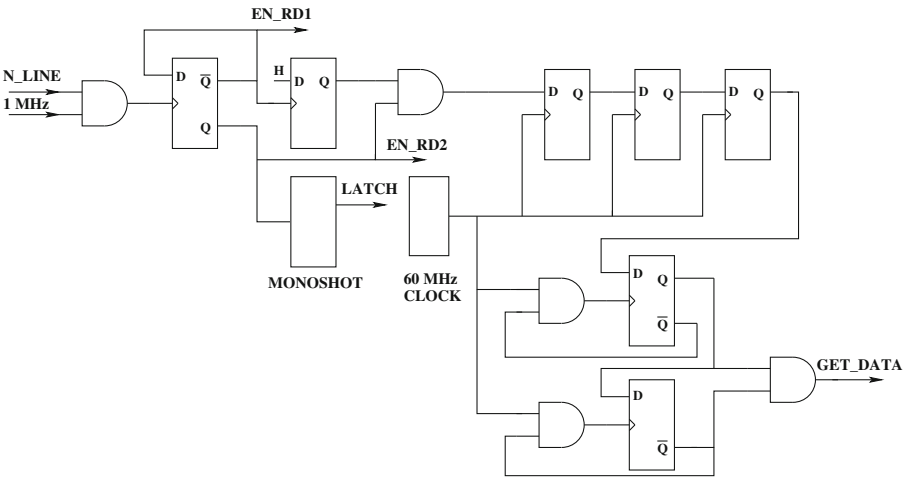

Fig. 2 Schematic of the control logic for G3TDC

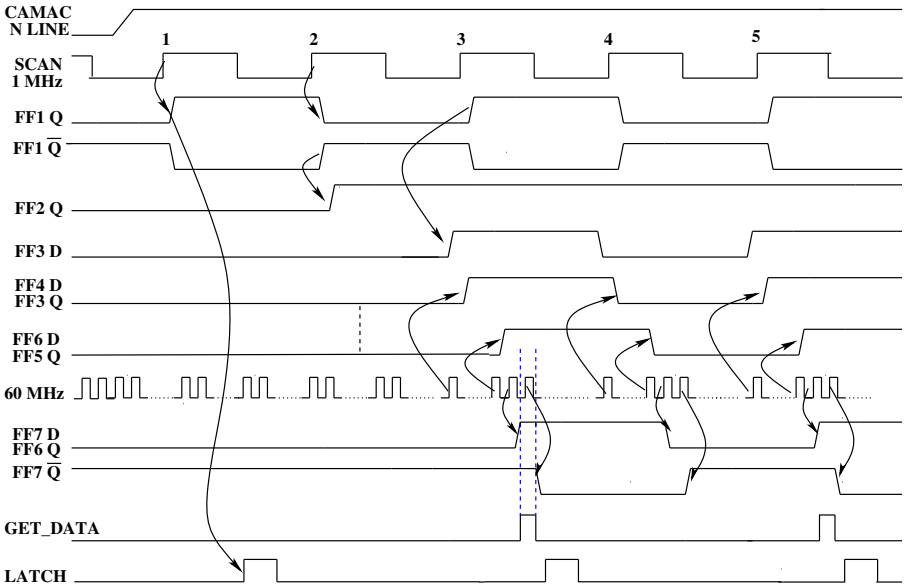

Fig. 3 Timing diagram for control logic of G3TDC

of time information, 6 bits for addressing a channel, 5 bits for addressing different modules) that are read as two 16 bit packets by the GRAPES-3 DAQ. This task is accomplished by using complementary outputs of FF1, named, EN_RD1 and EN_RD2, respectively, as shown in Fig. 2. The second SCAN clock also sets FF2 to a HIGH state for the duration of READ operation. The combination of remaining FFs and AND gates shown in Fig. 2, generates a GET_DATA signal that is synchronous with the trailing edge of 60 MHz clock, as shown by the 2nd waveform from bottom in Fig. 3. However, the leading edge of GET_DATA precedes 60 MHz clock without overlapping with the previous pulse in the train of 60 MHz pulses. This was the most critical requirement in the CONTROL UNIT, since the available time window was only 8.3 ns. A LATCH signal is generated immediately following the GET_DATA as shown by bottom waveform in Fig. 3, thus ensuring that the correct value of time is latched and recorded by the DAQ.

4 Comparative performance of TDCs

The G3TDC modules were extensively tested and calibrated prior to installation in the GRAPES-3 DAQ. Initially, the signals from several detectors were connected in parallel to the G3TDC as well as the Phillips or Hoshin TDCs for

a comparative field study of their performances. For the present study we have used six 16-channel TDC modules, each from Phillips and Hoshin for a total of 96 channels from the two manufacturer. We also used three G3TDC modules for a total of 96 channels.

It was observed that the time resolution (ps) of commercial TDCs displayed significant channel-to-channel variation and for some of the channels it also varied with time. To correct for these variations, a multi-channel calibration system was designed to measure the time resolution (TR) of individual channels in each TDC module. The calibration system employs six quartz crystal oscillators to provide stable clocks of known frequency. The 1st pulse in the pulse train was used as the START and the 2nd as STOP, for each channel in the TDC module being calibrated. Therefore, the time interval between these two pulses was 'T', where T is period of the oscillator. This procedure was repeated a hundred times. Thereafter, the 3rd, 4th, . . ., nth pulse, respectively, were used as STOPs, again repeated a hundred times for each delay. Thus, each TDC channel was calibrated a hundred times for the time intervals of T, 2T, 3T, . . ., nT. The six quartz crystals oscillators of frequencies 10, 16, 20, 25, 32, and 40 MHz were used. Typically ∼140 distinct time intervals were recorded during this calibration exercise over a time window of 1000 ns, thus ensuring a reasonably uniform coverage of this window.

As mentioned earlier, a total of three G3TDC, six Phillips and six Hoshin modules were used in the present study, amounting to a total of 96 channels for each of the three TDC types. The calibration results for one out of 96 channels from each of the three TDC types are shown in Fig. 4. The result from the G3TDC is shown in the top panel and a linear fit to this data yields a TR of 520.88 ps. Results from the Phillips and Hoshin TDCs are shown in middle and bottom panels, respectively in the same figure. A linear fit to data yield TRs of 199.8 and 285.2 ps for Phillips and Hoshin TDCs, respectively.

Next, the time difference between the measured delay and the linear fit was calculated. This time difference termed 'deviation' and represented by 'Δt' is shown as a function of delay in Fig. 5a for the G3TDC channel shown in Fig. 4a. The values of the Δt are uniformly distributed around a null mean. The root mean square (rms) Δt termed 'Δt_{rms}' is 82 ps. The deviation for Phillips channel is shown in Fig. 5b. Here, a large and systematic departure from linearity as a function of delay is observed. This behavior is seen in all Phillips channels that display a concave profile, although the actual magnitude varies from channel to channel. $\Delta t_{rms} = 603$ ps is calculated from the data shown in Fig. 5b. The Hoshin channel also showed a fairly large systematic non-linearity with a convex profile as shown in Fig. 5c and $\Delta t_{rms} = 298$ ps.

Next, we generated three distributions of TRs for each of the three TDC types separately, to get a measure of the spread in their magnitudes. These distributions were fitted to a Gaussian function and the fit parameters including the mean and standard deviation (SD) are shown in Table 1. The mean TR was 520.854 ps for the G3TDC, 199.52 ps for Phillips and 282.7 ps for

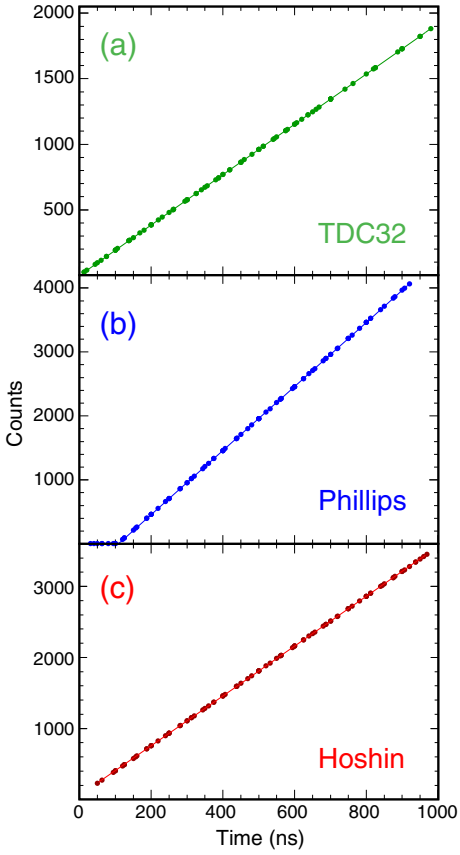

Fig. 4 Typical TDC calibration for, **a** TDC32 time resolution (TR) = 520.86 ps, **b** Phillips TR = 199.8 ps, **c** Hoshin TR = 285.2 ps

Hoshin TDCs. On the other hand, the magnitudes of SD for these three TDCs are radically different from each other and therefore, a somewhat unusual method for plotting these distributions was adopted. The minimum value of each distribution was adjusted to 1.2 ps by adding an appropriate offset. This procedure allowed all three distributions to be accommodated in the same panel, while using a log-log scale as shown in Fig. 6. The data are represented by the histograms and the Gaussian fit by dashed curves. Due to the procedure described above, the X-axis labeled in picoseconds does not represent the true mean of the distribution, however, the width does correspond to the data. Since, only the channel-to-channel variations are being investigated here, the above log-log representation indeed serves this limited purpose.

The narrowest histogram labeled 'a' corresponds to a TR of 96 G3TDC channels and a Gaussian fits the data rather well as seen from Fig. 6. The measured TR was 520.854 (Table 1) as against an expected value of 520.833 ps based on a frequency of 60 MHz. The small difference of four parts in 10^5 in the values of the measured and expected TRs is consistent with the accuracy of the

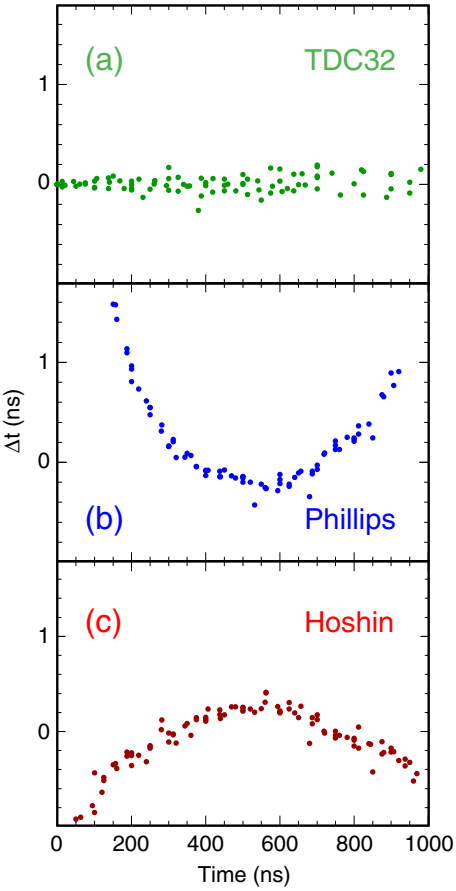

Fig. 5 Deviation from linearity obtained using TDC calibration for, **a** TDC32 $\Delta t_{rms} = 82$ ps, **b** Phillips $\Delta t_{rms} = 603$ ps, **c** Hoshin $\Delta t_{rms} = 298$ ps

frequencies of quartz oscillators used. Furthermore, TR of G3TDC channels are nearly constant as indicated by a SD of only 14 fs. In contrast the Phillips TDCs with a mean TR of 199.52 ps had a large spread with SD = 440 fs, nearly ∼30 times larger than the G3TDC (see Table 1), as seen from the plot labeled 'b' in Fig. 6. Finally, the Hoshin TDCs displayed the largest spread in TR with a mean of 282.7 ps (see Table 1) and SD = 3600 fs, nearly ∼260 times larger than the G3TDC, as shown by plot labeled 'c' in Fig. 6. Therefore, these studies clearly establish that the performance of G3TDC in reliably measuring the time is vastly superior than the two commercial TDCs studied here.

Table 1 TDC parameters

TDC type	Mean (ps)	S.D. (fs)
G3TDC	520.854	14
Phillips	199.52	440
Hoshin	282.7	3600

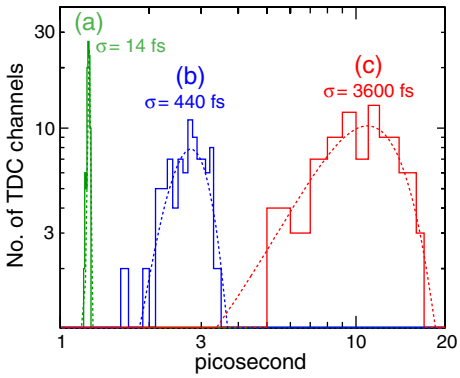

Fig. 6 Distributions of TDC time resolutions after setting mean = 1.2 ps. Histograms are for 96 channels and dashed curves are Gaussian fits for, **a** G3TDC, $\sigma = 14$ fs, **b** Phillips, $\sigma = 440$ fs, **c** Hoshin, $\sigma = 3600$ fs

According to the technical specifications, TDC32 has an rms time resolution of 0.2 ns, when operated at 60 MHz. However, in the START-STOP mode employed here, the measured time was obtained as a difference between a START and a STOP signal. Therefore, the effective rms time resolution is the quadratic sum of the two individual resolutions, $(0.2^2 + 0.2^2)^{0.5} = 0.28$ ns. The calibration data for a fixed delay for hundred events was used to generate a distribution of the TDC counts that is shown as a histogram in Fig. 7, after subtracting the mean of the TDC counts to center the distribution at zero. The rms width of this histogram is 0.49 counts and a Gaussian fit yields a nearly identical SD of 0.48 counts. Using a TR of 0.521 ns for the TDC32, yields an rms time resolution of $0.49 \times 0.521 = 0.26$ ns, in close agreement with the expected magnitude of 0.28 ns. Thus, we conclude that the G3TDC has performed exactly according to the technical specifications [21].

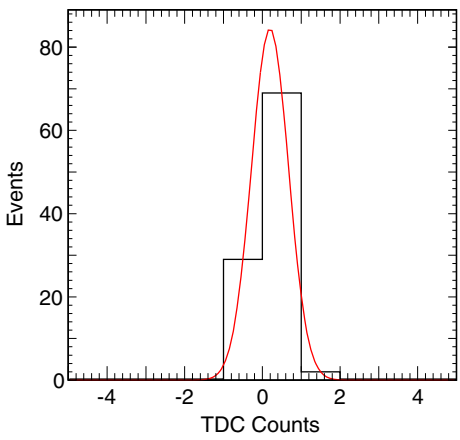

Fig. 7 Distribution of TDC counts for a fixed delay for 100 events, **a** histogram G3TDC data, rms = 0.49, **b** Gaussian fit, SD = 0.48

5 Time distribution of EAS particles

The TDC32 was designed with a built-in multi-hit capability and a double-hit resolution of only 15 ns as outlined in Section 2 [21]. In the discussions above, the multi-hit feature of this device was not explored. Here, this capability is exploited to measure the temporal structure of the particles in the EAS, and its dependence on the distance from the core. N_{sum} is defined as a sum of particles recorded in every GRAPES-3 detector triggered. Here the detector receiving a signal $\geq$40 % of a minimum ionizing particle with arrival time information from associated TDC channel is considered triggered for this purpose. N_{sum} turns out to be a good proxy for the primary energy of the EAS as shown below.

A total of 4.26×10^8 showers, recorded from January 1 to June 30, 2010 were analyzed. Only the EAS that triggered a minimum of 10 detectors were used for further analysis. An approximate position of the EAS core $\mathbf{R}_c$ was evaluated from the weighted mean of the locations $\mathbf{r}_i$ of the seven detectors with highest particle densities n_i, labeled H_7, whose weights equaled the densities in respective detectors as described in [28].

$$\mathbf{R}_c = \frac{\sum_{H_7} n_i \mathbf{r}_i}{\sum_{H_7} n_i} \tag{1}$$

The scintillator detectors in the GRAPES-3 array are shown as blue points in Fig. 8. A cut was applied on the location of the EAS core, to restrict it within an area that excluded a minimum of two outermost rings of detectors. The footprints of the cores of selected EAS are shown as red points. A total of 3.77×10^8 EAS, spread over an area of 1.27×10^4 m^2 survived this cut, during

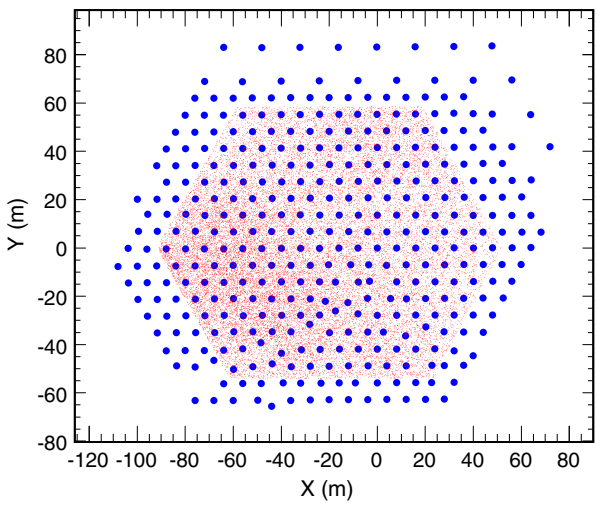

Fig. 8 The distribution of the cores of selected EAS incident on the GRAPES-3 array

a total live time of 160 d. The distribution of the number of EAS, 'N_{EAS}' with a particle sum of N_{sum} is shown as a histogram in Fig. 9, after multiplying by $N_{sum}^{2.5}$. Also shown on the same plot is a power law fit to the data in the range 50–3000 particles.

The frequency distribution of N_{sum} displays a power law behavior that may be approximated to $K \times N^{-\gamma}$. Here, K is a constant, and $\gamma = 2.58$. This value of 2.58 of spectral index may be compared with the values of 2.5 for the shower size spectrum [28] and 2.56 ± 0.04 for the density spectrum of the particles in EAS [29], measured earlier by us. The approximate equality of the spectral indices from three different methods indicates N_{sum} to be a good proxy for the primary energy of the EAS.

Next, we analyzed the multi-hit data from 106 detectors that were connected to the four G3TDC modules in the GRAPES-3 DAQ. To transmit the signals to the control room two different types of co-axial cables, namely, RG58 and 5D2V were used for 49 and 57 detectors, respectively. The transmission properties of the 5D2V cable are superior than the RG58 cable. Therefore, the data from 57 detectors that employ 5D2V cables were used for further analysis. For each detector, the events containing double-hits during a programmed window of 3000 ns were identified. The distribution of the time interval between the two hits in a double-hit event for detector numbered 234 is shown in Fig. 10. The sharp peaks in this figure are a result of the reflections of PMT signals in the 5D2V cable from detector 234 in the outdoor field to the Fan-Out, and from the Fan-Out to the G3TDC module in the control room. Next, we imposed a stringent cut on the level of reflection at <1.0 %, to select detectors for further analysis. Not surprisingly, only five out of 57 detectors passed this cut including detectors numbered, 199, 207, 230, 232 and 234. The performance of a detector in the reconstruction of EAS direction is unaffected even by a much higher level of reflection, but this stringent cut was imposed to analyze the double-hit data, that are far more sensitive to the level of reflections.

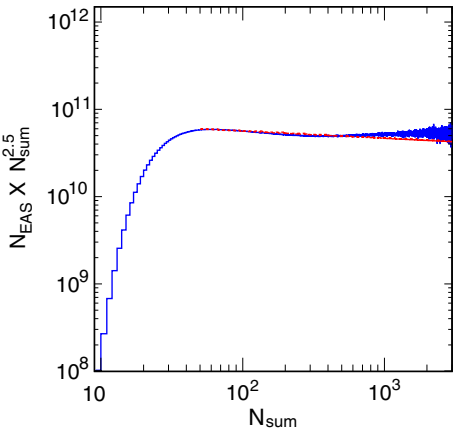

Fig. 9 Distribution of number of selected EAS 'N_{EAS}' multiplied by $N_{sum}^{2.5}$ as a function of 'N_{sum}'. Fit to data shown as *dashed line*, yields $N_{EAS} = K \times N_{sum}^{-\gamma}$ where $\gamma = 2.58$

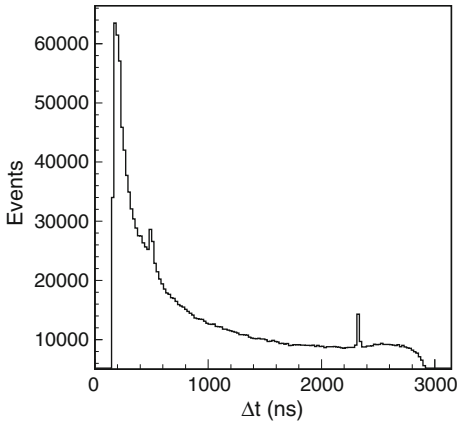

Fig. 10 Distribution of time intervals of double-hit events in detector 234. Reflection peaks are present at 500 and 2300 ns

The double-hit events in these five detectors were further classified into three categories, according to their distance from the shower core, namely, (a) 0–50 m, (b) 50–100 m, and (c) >100 m. Next, the distribution of the double-hit time intervals was obtained for the three ranges of core distances listed above. Since the time distributions for a given core distance range were very similar for all five detectors, their data were combined and are shown in Fig. 11. The distribution of double-hit time interval of 6.8×10^6 events for core distance 0–50 m is shown in Fig. 11a. The data were fitted with an exponential function and a constant background $N = A + B \exp^{(-\frac{\Delta t}{\tau})}$, here N is number of events, Δt time interval. τ, A, B are constants derived from the exponential fit.

In the GRAPES-3 DAQ, the discriminator outputs have a width of ∼150 ns as may be seen from the absence of events below this value in Fig. 10. Thus, the minimum recorded time interval always exceeds 150 ns. Since the width of the programmed window for G3TDC was set at 3000 ns, hence the maximum time interval can not exceed this value. With the above two limiting conditions, the data in Fig. 11a were fitted to an exponential and a constant background in the range 200–2700 ns. This yielded a time constant, $\tau = (363 \pm 36)$ ns. The distribution of time intervals for core distance of 50–100 m containing 3.4×10^6 events is shown in Fig. 11b. The data, when fitted to the same functional form in the range 200–2700 ns yielded a time constant, $\tau = (374 \pm 28)$ ns. Similarly, the distribution of events for core distances of >100 m containing 3.7×10^5 events is shown in Fig. 11c. This data, when subjected to the same fit gave a time constant, $\tau = (373 \pm 37)$ ns. Thus, within the limits of the accuracy of these measurements (at levels of ∼10 %), the time distributions for the above listed three distance ranges of EAS core appear to demonstrate very similar exponential profiles.

As mentioned earlier, the presence of sub-relativistic neutrons in an EAS could explain the delay profile observed in Fig. 11. In future, we plan to carry out extensive Monte Carlo simulations of neutron production in the EAS cores to obtain a significantly better understanding of their delay profile.

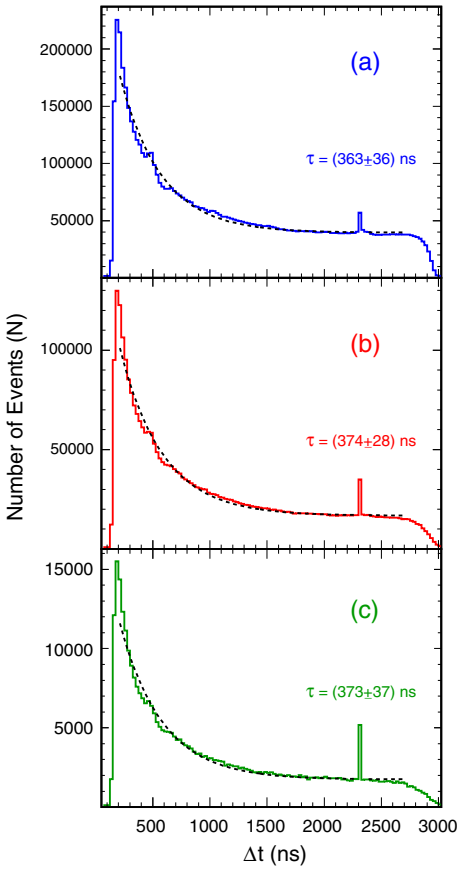

Fig. 11 Distribution of time intervals of double-hit events for core distance, **a** 0–50 m, **b** 50–100 m, **c** >100 m

These simulations would also focus on the observed weak dependence of the delay profile on the distance from the core up to a maximum of 100 m. With the planned upgrade of the GRAPES-3 array through the replacement of the remaining RG58 co-axial cables by vastly superior 5D2V cables and by using the multi-hit G3TDCs to record the data from each detector, we expect to detect a sizable number of neutrons in these detectors. The measurement of neutrons could potentially serve as an additional constraint on the models of hadronic interactions. It could also provide the GRAPES-3 array with an added capability to discriminate against the hadronic showers while searching for multi-TeV γ-rays from discrete sources.

6 Conclusions

A time to digital converter 'G3TDC' built on a CAMAC platform using the ASIC 'TDC32' developed at CERN has been subjected to extensive field tests over several years in the GRAPES-3 experiment at Ooty. The results of these

tests show that this device performed exactly as was originally designed. It also displayed exceptional long-term stability and negligible channel-to-channel variation in terms of time resolution. It was successfully operated in the TRIGGERED mode with a programmable window of 3000 ns. The analysis of the EAS data showed that small levels of reflections during transmission of signals over long co-axial cables could be easily detected. The multi-hit feature of this device could be used to measure the time structure of delayed particles in the EAS. This study clearly showed the presence of delayed neutrons that display an exponential profile with a time constant of about 370 ns. These neutrons could be detected following the passage of fast particles in the EAS front inside the same detector. Such detection offers the promising possibility of using neutrons for a better understanding of the hadronic interactions and possibly improving the capability for the detection of multi TeV γ-ray sources.

Acknowledgements We acknowledge the outstanding contributions of K. Manjunath and C. Ravindran in wiring, testing and installation of the G3TDC modules. We thank G.P. Francis, V. Jeyakumar, and K. Ramadass for their timely help in the fabrication of several mechanical components used and for the assembly of these modules. We also thanks P.K Nayak for his extensive help during the preparation of this manuscript. Stimulating discussions with S.R. Dugad deserve a special mention. This work is dedicated to the memory of our brilliant colleague, late S. Karthikeyan, who had made significant contributions to this as well as several other GRAPES-3 activities, prior to his tragic demise in a road accident.

References

1. Malkov, M.A., Drury, L.O.C.: Nonlinear theory of diffusive acceleration of particles by shock waves. Rep. Prog. Phys. **64**, 429–481 (2001)
2. Michel, F.C.: Magnetic structure of pulsar winds. Astrophys. J. **431**, 397–401 (1994)
3. Weekes, T.C.: Very high energy gamma-ray astronomy. Phys. Rep. **160**, 1–121 (1988)
4. Gupta, S.K., et al.: A design study of atmospheric Cerenkov radiation telescope for very high energy gamma-ray astronomy. Astrophys. Space Sci. **115**, 163–183 (1985)
5. Gupta, S.K., Tonwar, S.C.: Angular resolution of the Ooty EAS array based on UHE gamma rays from Her X-1. J. Phys. G: Nucl. Part. Phys. **17**, 1271–1277 (1991)
6. Alexandreas, D.E., et al.: Observations of shadowing of ultrahigh-energy cosmic rays by the Moon and the Sun. Phys. Rev. D **43**, 1735–1738 (1991)
7. Oshima, A., et al.: The angular resolution of the GRAPES-3 array from the shadows of the Moon and the Sun. Astropart. Phys. **33**, 97–107 (2010)
8. Atkins, R., et al.: Milagrito, a TeV air-shower array. Nucl. Instrum. Methods A **449**, 478–499 (2000)
9. Bassi, C., et al.: High altitude test of RPCs for the Argo YBJ experiment. Nucl. Instrum. Methods A **443**, 342–350 (2000)
10. Amenomori, M., et al.: Development and performance test of a prototype air shower array for search for gamma ray point sources in the very high energy region. Nucl. Instrum. Methods A **288**, 619–631 (1990)
11. Borione, A., et al.: A large air shower array to search for astrophysical sources emitting γ-rays with energies $\geq 10^{14}$eV. Nucl. Instrum. Methods A **346**, 329–352 (1994)
12. Aglietta, M., et al.: Results on candidate UHE gamma-ray sources by the EAS-TOP array (1989–1993). Astropart. Phys. **3**, 1–15 (1995)
13. Antoni, T., et al.: The cosmic-ray experiment KASCADE. Nucl. Instrum. Methods A **513**, 490–510 (2003)
14. Gallant, Y.A., et al.: Search for PeV γ-ray sources with the GAMMA experiment. In: Proc. 29th Int. Cosmic Ray Conf. Pune, vol. 4, pp. 85–88 (2005)

15. Gupta, S.K., et al.: GRAPES-3—a high-density air shower array for studies on the structure in the cosmic-ray energy spectrum near the knee. Nucl. Instrum. Methods A **540**, 311–323 (2005)
16. Greisen, K.: The extensive air showers. Prog. Cosmic Ray Phys. Ed: J.G. Wilson **3**, 1–144 (1956)
17. Linsley, J.: Sub-luminal pulses from cosmic-ray air showers. J. Phys. G: Nucl. Phys. **10**, L191–L195 (1984)
18. Erlykin, A.D.: The neutron 'thunder' accompanying the extensive air shower. arXiv: hep-ph/0701179v1, pp. 1–12 (2007)
19. Antonova, V.A., et al.: Anomalous time structure of extensive air shower particle flows in the knee region of primary cosmic ray spectrum. J. Phys. G: Nucl. Phys. **28**, 251–266 (1984)
20. Hayashi, Y., et al.: A large area muon tracking detector for ultra-high energy cosmic ray astrophysics—the GRAPES-3 experiment. Nucl. Instrum. Methods A **545**, 643–657 (2005)
21. Christiansen, J.: 32 Channel general purpose Time to Digital Converter. CERN/ECP-MIC Ver. 1.0 January 1, pp. 1–57 (1997)
22. http://www.lecroy.com/lrs. Accessed 1 Aug 2012
23. http://www.phillipsscientific.com. Accessed 1 Aug 2012
24. http://www.kagaku.com/hoshin/english.html. Accessed 1 Aug 2012
25. Gupta, S.K., et al.: Performance of CAMAC TDC and ADC in magnetic field. Nucl. Instrum. Methods A **400**, 428–434 (1997)
26. Ljuslin, C., Christiansen, J., Marchioro, A., Klingsheim, O.: An integrated 16-channel CMOS time to digital converter. IEEE Trans. Nucl. Sci. **41**, 1104–1108 (1994)
27. Santos, D.M., et al.: A CMOS delay locked loop and sub-nanosecond time-to-digital converter chip. IEEE Trans. Nucl. Sci. **43**, 1717–1719 (1996)
28. Tanaka, H., et al.: Studies of the energy spectrum and composition of the primary cosmic rays at 100–1000 TeV from the GRAPES-3 experiment. J. Phys. G: Nucl. Part. Phys. **39**, 025201 (16pp) (2012)
29. Mohanty, P.K., et al.: Measurement of some EAS properties using new scintillator detectors developed for the GRAPES-3 experiment. Astropart. Phys. **31**, 24–36 (2009)